Effects of Architectural Variability on the In-Plane Strength of a Woven Ceramic Matrix Composite

M. B. GOLDSMITH, B. V. SANKAR and R. T. HAFTKA

ABSTRACT

Woven ceramic matrix composites such as SiC/SiC are candidate materials for future hypersonic vehicle systems such as thermal protection systems and aero-propulsion systems. However, randomness in woven ceramic matrix composite architecture has been found to cause large variability in stiffness and strength. The effect of varying architecture on the variability of in-plane tensile strength is studied using the Brittle Cracking Model for Concrete in the commercial finite element software, Abaqus. A maximum stress criterion is used to evaluate failure, and the stiffness of failed elements is gradually degraded such that the energy required to open a crack (fracture energy) is dissipated during this degradation process. While the varying architecture did not create variability in the in-plane stiffness, it does contribute significantly to the variability of in-plane strength as measured by a 0.02% offset method. Applying spatially random strengths for the constituents did not contribute to variability in strength as measured by the 0.02% offset. However, if the strength varies in larger clusters (rather than completely randomly), there are some variations in strength. While the architecture causes a larger amount of variability than random constituent strength, the architecture and local constituent strength play a synergistic role in determining the strength of the composite.

INTRODUCTION

Background

Woven ceramic matrix composites are of current interest for harsh thermo-structural conditions such as those encountered by hypersonic vehicle systems and turbine engine components. Randomness in the tow architecture, as well as the randomly shaped and spaced voids

Marlana Goldsmith, University of Florida, Gainesville, FL
Bhavani Sankar, University of Florida, Gainesville, FL
Raphael Haftka, University of Florida, Gainesville, FL

that are produced as a result of the manufacturing process, are features that contribute to variability in stiffness and strength.

ARCHITECTURAL VARIABILITY

The effects of architectural variability have been recognized as important for understanding how structures fail under various loading conditions [1], [2]. There is a large body of work with various attempts at capturing the effects of architectural variability for polymer matrix composites (PMCs) [3]–[5]. Others are working on this problem for CMCs which may behave quite differently given the differences in processing techniques [6]–[9]. It is typical to limit the various types of architectural variability being studied in order to keep the problem tractable. For example, Woo and Whitcomb [5] studied the effects of tow misalignment and Chang [3] investigated tow geometry changes as a result of draping. While some limit the amount of variability in properties studied, early work at NASA included probabilistic analysis of numerous aspects of variability. Some of these variables included constituent mechanical properties and strength, volume ratios, and architectural variability such as ply misalignment [10]. Similar work was done by Desplentere for 3D woven composites in which detailed X-ray images were used to quantify architectural variability [1].

PROGRESSIVE DAMAGE

When considering the failure and strength of composites, both progressive and non-progressive damage methods used. Non-progressive methods such as those that use first element or first ply failure are simple and appropriate for some analyses, especially in early stages of design (e.g. [11], [12]). However, they do not provide much insight into the progressive nature of failure. While many methods have been proposed for modeling the progressive damage and failure in composites, there are two unifying topics. These include an element or ply discount approach which is typically stress-based, continuum damage mechanics, and fracture mechanics. Each has their strengths and limitations, and their usefulness depends on the application.

In the above mentioned methods, analysis begins with a comparison of stress, either in an element or in a ply, to the strength of the material. The difference lies in the degradation model. Usually an incremental-iterative technique is used, which means an iteration is performed at each load or displacement increment, but small increments in between are also used to ensure stability. Failure criteria are evaluated at each increment and material properties are degraded by a factor determined by the analyst if failure is detected. Karkkainen, Sankar, and Tzeng [[13]], as well as many others make use of this method., Work by authors such as Ochoa and Engblom [14] and Knight [15], used a process in which, for each load increment the lamina stresses were checked for failure based on several different failure criteria that were related to the mode of failure. If the stress in the fiber direction exceeds the allowable stress, the stiffness in the fiber-direction is degraded. A similar process was completed for a plane woven composite in work by Blacketter et.al. [16].

Continuum damage mechanics methods also involve checking the failure criteria, and degrading material properties. However, it is usually done in a way that represents the physics of the damage occurring. Continuum damage mechanics typically involves the use of a damage variable which introduces damage by degrading the stiffness

tensor on the basis of a damage law [17], [18]. The way in which the stiffness matrix is degraded varies, and there is no universal method that is appropriate for all materials or all applications. The choice of damage evolution may come from experimental data fitting which limits capabilities in virtual design of a material [19]. However, current predictive methods typically require some calibration to experiments and have been shown to work very well. In work by Pineda et al., Schapery Theory which is based on the energy potential required for structural changes to occur is used [20]. Other models are based on relationships due to observed cracking or fracture. For example, Talreja [21] has developed a method in which crack density can be related to damage evolution.

Another method of determining damage evolution is based on the fracture mechanics concepts of fracture toughness and strain energy release rate of the material [22], [23]. This method is valuable for this work because it is derived from information about material properties (fracture toughness and strain energy release rate) that can generally be found in the literature. Since it is a popular method, it is also already implemented in many finite element analysis packages, including Abaqus which has a model titled Brittle Cracking for Concrete (BCC) [24]. This model is based on early work that was done for concrete, but it can be applied to brittle materials in general [25]. It is similar to the model by Barenblatt that used traction separation laws to define the damage [26]. In the BCC model, elements that are failing can be thought of as cracks. When the maximum tensile stress is reached, the stress does not become zero suddenly, but gradually decreases as the crack width increases (the element length increases). The amount of energy needed to open the crack, and the way in which the energy dissipates dictates the post-peak softening behavior. This method also has similarities to cohesive zone modeling [27]. The key advantage offered by implementing the continuum damage mechanics method over cohesive zone modeling is that the location of the crack does not need to be known a priori.

Objectives of Current Work

Previous work by the authors demonstrated that modeling the voids is important when determining the transverse stiffness [28], [29]. The in-plane stiffness properties were not as sensitive to changes in the architecture and were generally related to the void volume fraction. The objectives of the work described here are to assess the amount of variability in the in-plane tensile strength measured by a 0.02% offset method for three cross sections with varying architecture and begin to understand which aspects of the model need to include variability. A smaller (or larger) strain offset can be used, but similar results will be obtained when comparing strengths relative to one another. The composite can still sustain substantial loads after this point, but the failure requires inclusion of damage mechanisms such as environmental effects, which are beyond the scope of this work. The variability in strength due to architectural variability is compared to the effects of using random strength in the constituents (a more common variable to randomize). These effects are studied by using a progressive damage model that allows the observation of damage initiation and propagation.

DETAILS OF FINITE ELEMENT MODEL AND PROGRESSIVE DAMAGE

It was desired to find a readily available material model which could be used, along with appropriate assumptions, to evaluate the importance of modeling the varying architecture and the varying strength of the constituents. There are several types of damage initiation and evolution models in commercial FE software, e.g. Abaqus [24]. The majority of them are applicable to metals in which the post-peak softening behavior is ductile rather than brittle. However, there are a few models which allow the simulation of brittle behavior. The majority are applicable to metals in which the post-peak softening behavior is ductile rather than brittle. However, there are a few models which allow the simulation of brittle behavior. One is the Brittle Cracking Model for Concrete which uses Rankine (maximum stress) failure criterion. The material property degradation uses concepts derived from fracture mechanics which determines the post-peak softening behavior based on the energy required to open a crack [25]. The model was developed for concrete, but is found to be applicable to some other brittle materials, also.

Since we are interested in the yield strength and not the ultimate tensile strength, failure and damage in the longitudinal tows are not modeled. While ceramics do not typically exhibit a yielding type of behavior, CMCs do, due to the fiber reinforcements. Several researchers have shown experimentally that in the region of the stress-strain curve that lead up to yield strength, damage occurs predominantly in the inter-tow matrix and in the matrix of the tows. Lamon [30] outlines the failure process in a plain woven CMC as follows. First, cracks initiate at inter-tow pores (macropores) at strains between 0.025% and 0.12%. Then cracks begin to form in the transverse tows between strains of 0.12% and 0.2%. Lastly, cracks are seen in the longitudinal tows for strains larger than 0.2%. The strains at which these failure modes occur in the 5HS SiC/SiC composite are different, due to the different weave and manufacturing process, but the general evolution of damage is similar. This is validated by the work of Morscher [31] in which damage was detected using acoustic emission (AE) techniques on a 5HS CVI SiC/SiC composite, almost identical to the one studied here. The first AE event occurred at small strains (less than 0.05%) and corresponded to formation of microcracks. The large AE event was related to large matrix cracking and crack bridging through the tows which occurred around a strain of 0.05%. These experimental observations indicate that if the yield strength is the strength of interest, modeling damage in matrix and transverse tows is sufficient.

Material Properties

STIFFNESS AND DETERMINISTIC STRENGTH

The Young's moduli, shear moduli, and Poisson's ratios of the matrix and longitudinal tows are the same as that prescribed for the stiffness analysis in Table 1. However, the Brittle Cracking Model in Abaqus can only be used for isotropic materials. Since the tow properties are transversely isotropic, and they are only being loaded in the transverse direction, the tows can be modeled as an isotropic

material with properties equal to those of the transverse direction (E = 106 GPa, ν = 0.21).

Strength properties of the constituents are less straight-forward and are not widely found in the literature. However, one of the objectives of the work is to determine which characteristics of the model need to be varied in order to capture variability. Therefore, determining reasonable properties based on experience and pertinent assumptions with the aid of limited experimental data is appropriate. Note that discussion of stochastic strength properties follows this discussion.

The first assumption made is that the transverse tows fail because of matrix cracks. The fibers in the transverse tows do not carry any significant stress when the loading is in the longitudinal direction. Therefore, the strength of the tows can be found similarly to the matrix. Then, Morscher observed that in a 5HS CVI SiC/SiC composite, the large acoustic emission occurred at 0.05% strain [31]. At this time, there were significant cracks in the matrix and transverse tows. We can then assume that if the local strain is approximately equal to the global strain, then the matrix too may fail at a strain of approximate 0.05%. We know that the local strain everywhere is not equal to the global strain, but it is not an unreasonable approximation.

Figure 1 is a composite model at a global strain of 0.05%. The area marked in red corresponds to local strains of 0.04% to 0.06%. The blue elements (lower strains) and grey elements (higher strains) are the only ones outside of this range. Therefore, we assume that the global failure strain can be related to the local strain. Then we can use the relationship $\sigma_f = \varepsilon_f E = 0.0005E$ to determine that the failure stress of the matrix is 252 MPa and the failure stress of the transverse tows is 53 MPa. The transverse tow strength may seem low. However, if one compares the value to that of the matrix strength, and considers that the fibers could have a weakening effect in the transverse direction, the value is not unreasonable. There are no experimental results to verify the strength, but work by Evans and Zok [32] also indicate that the result is reasonable. Evans and Zok cite a transverse tow strength of 10 MPa for another CMC, SiC/CAS (calcium aluminosilicate) [32]. A summary of the stiffness, strength, and fracture energy properties discussed here and continued below are found in Table 2.

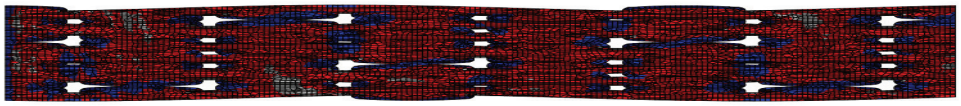

Figure 1. Finite element model at a global longitudinal strain of 0.05%. The red elements have a strain of 0.05 ±0.01%, while they blue elements and grey elements lie below and above this range, respectively.

Table 1. Actual constituent material properties

	Transverse Tow	Longitudinal Tow	Matrix
E_1 (GPa)	106.0	259.0	420.0
E_2 (GPa)	259.0	106.0	420.0
E_3 (GPa)	106.0	106.0	420.0
v_{12}	0.21	0.21	0.17
v_{13}	0.21	0.18	0.17
v_{23}	0.18	0.21	0.17
G_{12} (GPa)	41.4	41.4	179.5
G_{13} (GPa)	41.4	42.5	179.5
G_{23} (GPa)	42.5	41.4	179.5
α (10^{-6}/°C)	4.6	4.6	4.7

Table 2. Properties used for the BCC model: Young's modulus, Poisson's ratio, strength, strain at maximum tensile stress, fracture energy, and displacement at failure for the transverse tows and matrix

	Transverse Tow	Matrix
E (GPa)	106.0	420.0
v	0.21	0.21
σ_f (MPa)	53.0	252.0
ε_f	0.05%	0.05%
G (N/m^2)	21.0	21.0
u_u (μm)	8.0	1.7

STOCHASTIC STRENGTH OF THE TRANSVERSE TOWS AND MATRIX

Ceramic failure is especially stochastic due to its sensitivity to flaws in the material. The strength of a ceramic is generally described by a two parameter Weibull distribution. The parameters are the scale parameter λ, and the shape parameter (frequently referred to as the Weibull modulus) m. These parameters can be used to determine the mean and standard deviation of the distributions using the equations

$$\mu = \lambda\Gamma(1+\frac{1}{m}) \tag{1}$$

$$\sigma = \sqrt{\lambda^2\Gamma(1+\frac{2}{m}) - \mu^2} \tag{2}$$

where Γ is the gamma function. Estimations of the Weibull parameters for the inter-tow matrix and transverse tow matrix were made by Lamon et al. [33], using finite element analysis that included probabilistic information about the constituents. The scale parameter and shape parameter for the matrix were found to be 291 MPa and 4.9, respectively. The scale parameter and shape parameter for the transverse tow matrix were 120 MPa and 4.9, respectively. For the given values, the scale parameter has a larger influence on the calculated mean than the shape parameter whereas the shape parameter has a large influence on the calculated standard deviation or amount of variability. The purpose of using Lamon's estimates is to obtain an approximation for the variability of the composite's

constituents. The mean strength (approximately 10% lower than Lamon's mean strength, mostly due to differences in material volume fractions) has already been decided by deductions described in the previous section. Therefore, the shape parameter m from the work cited (m = 4.9) will be used in combination with our previously determined mean strength. Using Equations 1 and 2, the corresponding scale parameter of the Weibull distribution and standard deviation can be determined (see Table 3). A plot of the cumulative distribution function and probability distribution function are given in Figures 2 and 3 to provide a visual representation of the variability in strength.

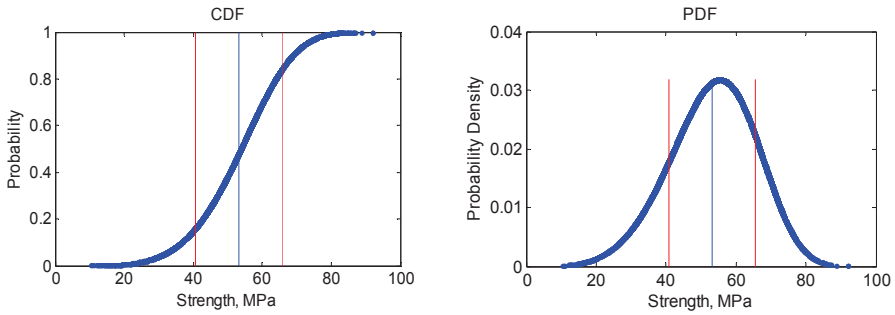

Figure 2. Cumulative distribution function and probability distribution function plots of the Weibull distribution of transverse tow strength. The straight blue line and 2 red lines mark the mean and one standard deviation from the mean, respectively.

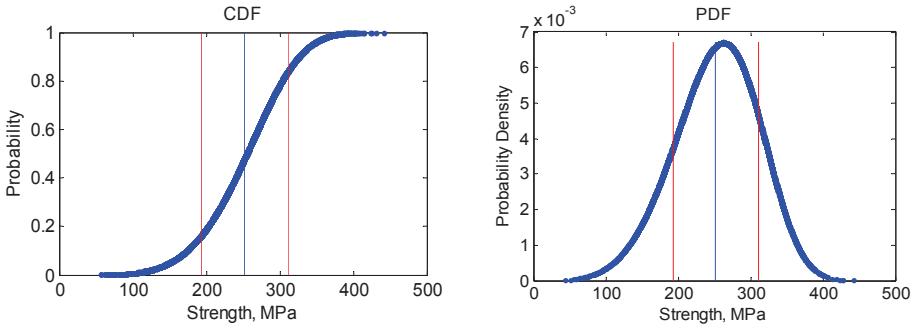

Figure 3. Cumulative distribution function and probability distribution function plots of the Weibull distribution matrix strength.

Table 3. Weibull parameters of two parameter Weibull distribution and the corresponding mean and standard deviation

	Transverse Tow	**Matrix**
Scale parameter, λ (MPa)	58.0	275.0
Shape parameter, m	4.9	4.9
Mean of distribution, μ (MPa)	53.0	252.0
Standard deviation, σ (MPa)	12.0	59.0

DAMAGE EVOLUTION AND FRACTURE ENERGY

This section explains the physics of the damage evolution after an element reaches its maximum allowable stress how the fracture energy of the constituents was selected. The Brittle Cracking Model for Concrete available in Abaqus combines finite element analysis with fracture mechanics concepts [24], [25]. Abaqus uses a smeared crack approach which means that cracks are not explicitly

modeled, but cracks affect the stress of the element. The crack is formed perpendicular to the direction of the maximum principal stress.

Hillerborg's model is illustrated in Figure 4 and described as follows. The crack propagates when the principal stress at the crack tip is equal to the failure stress of the constituent (σ_f). The stress in the element then begins to decrease with increasing crack opening u_c, as illustrated in Figure 5. When $u = u_u$, the stress is zero and the element can no longer carry any load. The area under the stress-displacement curve corresponds to a microcrack zone where there is stress to be overcome by opening the crack. The energy required to open the crack, or fracture energy, can then be used to describe how the stress changes with crack opening displacement, after the failure stress has been reached. The fracture energy can be written as

$$G = \int_0^{u_u} \sigma du \tag{3}$$

The shape of the stress-displacement curve is not limited to that of Figure 5. A curve generated experimentally can be used, or a different assumed post-peak softening behavior, as appropriate for the application. Since ideally a brittle material will fail rapidly (such that the stress drops to zero at the ultimate strain or in other words, there is no gradual softening), a simple linear degradation is appropriate and Equation 3 can be simplified to

$$G = \frac{1}{2}\sigma_f u_u \tag{4}$$

In addition to minimal experimental data being available for strength values, information about the fracture energy is not readily available either. Given the relationship of fracture energy to fracture toughness for plane stress and knowing that the typical fracture toughness for SiC is between 3-5 $\text{MPa}\sqrt{\text{m}}$ [34] we can estimate the fracture energy to be approximately

$$G = \frac{K_I^2}{E} = \frac{\left(3\times10^6\right)^2}{420\times10^9} = 21\frac{\text{J}}{\text{m}^2} \tag{5}$$

Fracture energy values of 15-25 J/m^2 have been cited by NIST (National Institute of Standards and Technology) for SiC, so the above approximation falls within a reasonable range [35]. The properties cited above are related to a SiC matrix. Similar properties were not available for the tows. Since the transverse tows fail due to matrix damage, the same fracture energy was assumed for the tows. Due to the failure stress of the tows being lower than that of the matrix, the slope of the post-peak softening behavior will be shallower, implying a larger displacement or strain to failure. However, the strain to failure is still small.

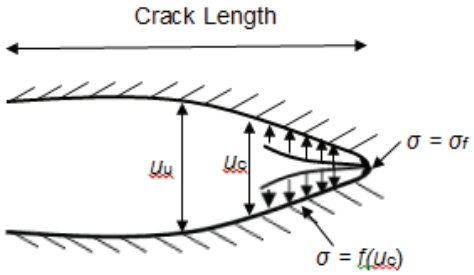

Figure 4. Illustration of variables used to describe damage evolution. σ_f is the maximum allowable stress, u_c is the crack opening displacement, and u_u is the crack opening displacement at failure.

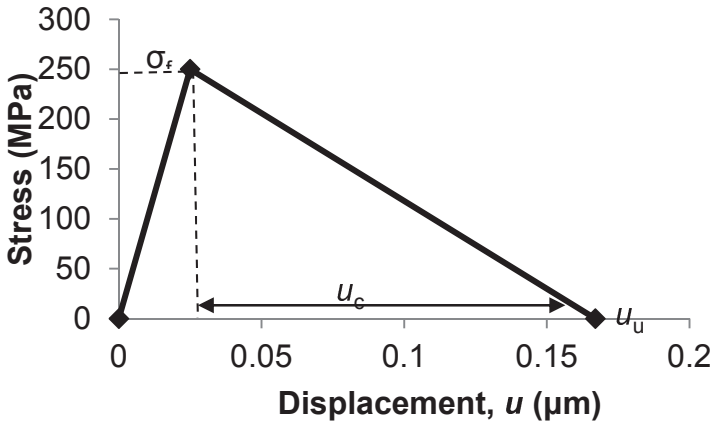

Figure 5. Sample stress-displacement curve illustrating the variables used to describe the damage evolution. Note that the area under the curve is the fracture energy.

Loads, Boundary Conditions, and Elements

The analysis considered in this study is a uniaxial displacement-controlled tensile test in the longitudinal direction on a cross section approximately 890 μm long with a thickness of 250 μm. The boundary conditions are illustrated in Figure 6. The right side of the composite (perpendicular to the loading direction) is prescribed a displacement. The left side is on rollers, free to move in the 3-direction, but remains straight with respect to the 1-direction. The boundary conditions on the edges parallel to the loading direction are free.

The displacement increments were not uniform for the entire analysis because of the computational expense. Instead, the first three steps (before damage typically begins), and last five (after onset of non-linearity) were in increments of 0.5 μm and 0.75 μm, respectively. The 23 steps in between were incremented by 0.15 μm. The final total strain of the composite was approximately 1%. Beyond this strain it becomes important to model damage in the longitudinal tows. Additionally, it is likely that environmental effects would start to play a major role as cracks have typically formed on the matrix surface.

The elements used for the strength analysis are a mix of plane stress 4-node quadrilateral elements and 3-node triangular elements. The plane stress elements allow the uniaxial tensile test to be simulated (no stress in the 2-direction). A more complete understanding of the effects of architecture should be obtained by using 3D models in future work.

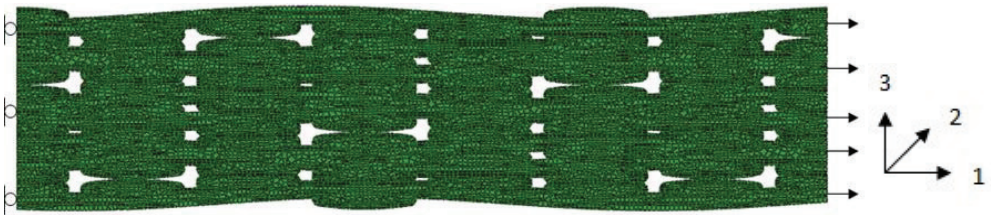

Figure 6. Boundary conditions for uniaxial tensile displacement-controlled loading

DESCRIPTION OF DAMAGE ANALYSIS CASES AND RESULTS

Effects of Varying Architecture on Strength

The first objective was to assess the impact of varying architecture on the strength of three different cross sections of the 5HS CVI SiC/SiC composite. The cross sections are taken from micrographs of the composite found in Figure A-1. The largest difference between the cross sections is the size and distribution/location of voids. The tow properties (tow width, tow height, tow spacing) have similar statistical distirbutions between each specimen as discussed in detail in Goldsmith, et al. [29].

The stress-strain curve based on the finite element results is shown in Figure 7 along with an experimental result on a similar, but slightly different material (different ends per inch used in manufacturing and different fiber volume fraction) from Morscher et.al. [31]. Therefore the stiffness is higher (due to differing constituent volume fractions), but the failure characteristics are the same in terms of when damage is observed, and the global strain in which the stress-strain relationship becomes nonlinear is also the same. Damage initiates in areas of high stress concentration in the matrix (near the voids, and between the tows on the surface, shown in Figure 8, and labeled as Point 1 in Figure 7). This point would likely correlate to the first acoustic emissions (AE) event discussed by Morscher, which was an AE event that signaled some degree of damage, but occurred before an onset of non-linearity in the stress-strain curve [31].

The onset of non-linearity in the stress strain curve begins around a strain of approximately 0.04%. At this point, damage has initiated in much of the matrix and the tows, shown in Figure 9 and labeled as Point 2 in Figure 7. Then, at the 0.02% offset, a significant amount of damage has occurred and many elements have completely failed, shown in Figure 10 and labeled in Figure 7 with the 0.02% offset line. Note that the longitudinal tows will always appear undamaged since damage is not being modeled in those elements. The observations made regarding when and where failure occurred was similar to those found by Mital et.al. [36]. They also observed failure initiating near tows and voids. However, they did not observe variability in the stress-strain behavior for the same cross sections used in this work. This is likely because progressive failure was not considered and instead the behavior after failure was perfectly plastic. As the constituents fail, the load-bearing capabilities decrease, and this plays an important role in the strength of the composite.

Using a 0.02% yield offset method as discussed previously, the variability in strength between the three cross sections is approximately 20 MPA or 17%. The variability in stiffness was approximately 5%. Damage is more dependent on local

phenomena and areas of high stress concentrations can decrease the strength significantly, especially when the elements lose load-bearing capabilities; whereas the stiffness involves averaging the stresses which effectively smears the effects of local phenomena. It is not clear exactly what aspects of the architecture cause the variability in strength, but for all cases, damage initiates near voids and in between tows that are close together on the surface.

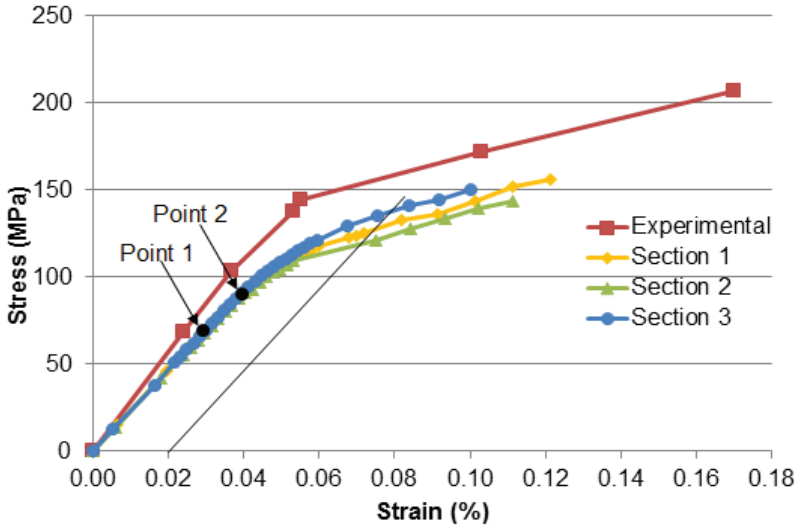

Figure 7. Stress-strain curve of three models with varying architecture compared to one experimental model of a slightly different material. Point 1 corresponds to damage onset. Point 2 corresponds to approximate onset of non-linearity. The 0.02% offset is also labeled. The experimental result is for a material with a higher initial stiffness [31].

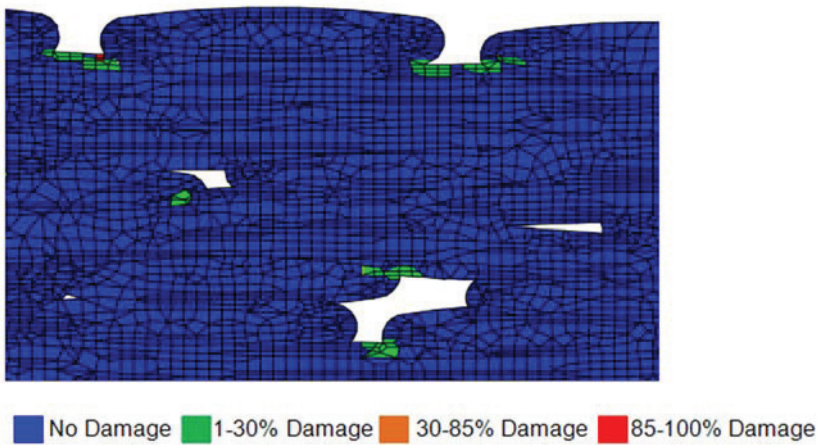

Figure 8. Zoomed in image of cross section 1 corresponding to damage onset labeled in Figure 7 as Point 1.

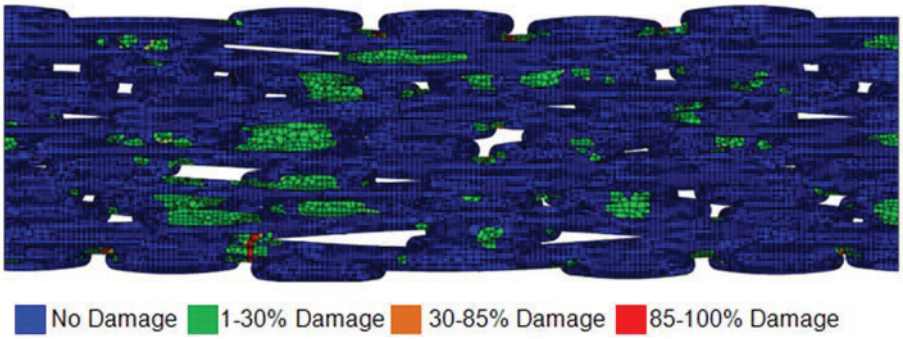

Figure 9. Image of cross section 1 corresponding to approximate onset of non-linearity labeled in Figure 7 as Point 2.

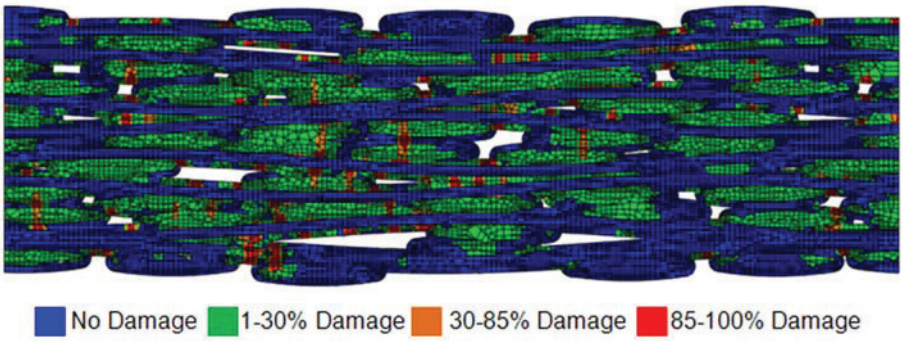

Figure 10. Image of cross section 1 corresponding to 0.02% yield offset labeled in Figure 7 with a black line

Effects of Varying Constituent Strength on Composite Strength

After varying the architecture, a varying constituent strength was applied. The strengths were chosen based on the Weibull distributions discussed previously. Computational limitations prevented each element from having a unique strength. Instead, each strength was assigned to 75 elements (with 7500 elements, this would imply 100 different strengths applied to groups of 75 elements). The elements in the group of 75 were distributed randomly so that 75 elements of the same strength were not bordering each other. Three different sets of strengths were tested (distribution of strengths drawn three separate times).

When generating random strengths, the mean of the distribution can vary from the distribution mean (with 100 samples the sample means will have standard deviations of about 10% of the distribution standard deviation or about 2.5%, see Table 3). In order to ensure that variability in the mean strength of the samples, we rejected samples whose mean strength of one the constituents exceeded ±3% of the distribution mean strengths (252 MPa for the matrix and 53 MPa for the transverse tows). Two additional deterministic analyses with the strength of the matrix increased by one standard deviation and decreased by one standard deviation were completed in order to determine how much of the variability in strength found was due to the change in the mean or actually due to the variable strength. A 23% change in the deterministic strength resulted in a 9% change in 0.02% offset strength. The change in offset strength due to the mean is found by linear interpolation. Table 4 summarizes the expected change in strength due to the

different mean strength of the distribution, compared to the actual change in strength.

For each of the three varying strength distributions in the three architectural models, there was almost no variability in the offset yield strength (less than 0.5%). The results are plotted in Figures 11-13. With the exception of cross section number 3, the yield strength did not change with respect to using a deterministic strength either. As indicated by Table 4, cross section 3 is the only cross section that indicated variability in strength due to the variable distribution (the expected change in strength due to the mean is smaller than the change in strength found). In all of the models there are areas of high stress concentration due to the voids. Failure begins near these points, and eventually occurs, at least to some degree, in most other areas of the composite. The initiation of damage may happen at a lower global strain due to an area of lower strength, but when the strain becomes large enough, a significant amount of failure is going to occur everywhere. It is not yet clear what causes cross section 3 to have a variation in yield strength. The variation is low (4%), but it is still higher than the other models. One hypothesis is that aspects of the architecture lead to more areas with large stress risers and this may increase the chance that weak elements and high stress concentrations will occur together as compared to the case in which the strength is deterministic. However, it is difficult to discern precisely which aspects of the architecture yield higher stress concentrations. Generally it appears that damage occurs near voids, and when tows are close together on the surface. Since it is difficult to visualize the concept close to the yield offset, it is illustrated at a smaller strain. Figure 14 shows cross section 1 with a deterministic strength and the randomly distributed strength. The areas in which damage initially evolves in the deterministic model are very similar to those in the randomly distributed strength model, with the exception of 2 spots highlighted in red. In cross section 3, the areas in which damage evolves are more numerous than at the equivalent strain in the deterministic model shown in Figure 15. The areas circled in red highlight areas in which elements have completely failed (or come very close to doing so) in the random model, but not the deterministic model.

Instead of the strengths being completely randomly distributed, it is also possible that the local strength manifests in clusters. There is no data to show whether this is the case, but if it does create some additional changes in the damage, it may be worth investigating. In order to test the effects of clusters, two models were used. The first one had 10 clusters of matrix strengths, and the variability in tows was the same as that applied in the initial models previously described. The second one had 10 clusters of tow strengths, with randomly varying matrix strength. The clusters were chosen such that they were layered through the thickness, numbered with cluster 1 at the bottom and cluster 10 at the top. Cluster 1 and cluster 5 of the matrix are highlighted in Figure 16. The strength of each cluster can be found in Table 5.

When the tows were clustered, the yield offset strength still did not change. However, when the matrix was clustered, the strength increased by approximately 4%. This is not large, but it is worth investigating why this may occur. If we observe the regions that have failed between the deterministic model, and the matrix clustered model, we see that for the same applied displacement, damage did not initiate in at least two major spots. In the deterministic model at the top of

Figure 17, we see that damage occurred near a void at the top and bottom of the composite, and we can see approximately where a crack would occur through the thickness. In the clustered model shown at the bottom of Figure 17, damage does not occur at the same time, or to the same degree. If we look at the strength of the matrix in those two regions in Table 5 (Cluster 2 and Cluster 9), we see that the strength is much higher than the deterministic strength of 252 MPa. If in this clustered model the points near the voids were especially weak, we can imagine that the amount of damage through the thickness would increase, resulting in a lower strength. The tows are not as sensitive to the local strength, likely because the failure of them is less dependent on the stress concentrations cause by the voids.

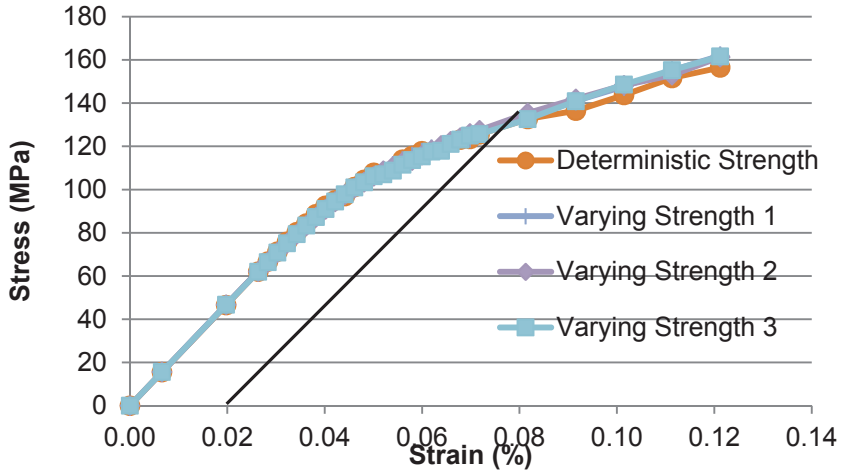

Figure 11. Stress-strain curves of cross section 1 with the deterministic strength and three different sets of strengths drawn from a Weibull distribution

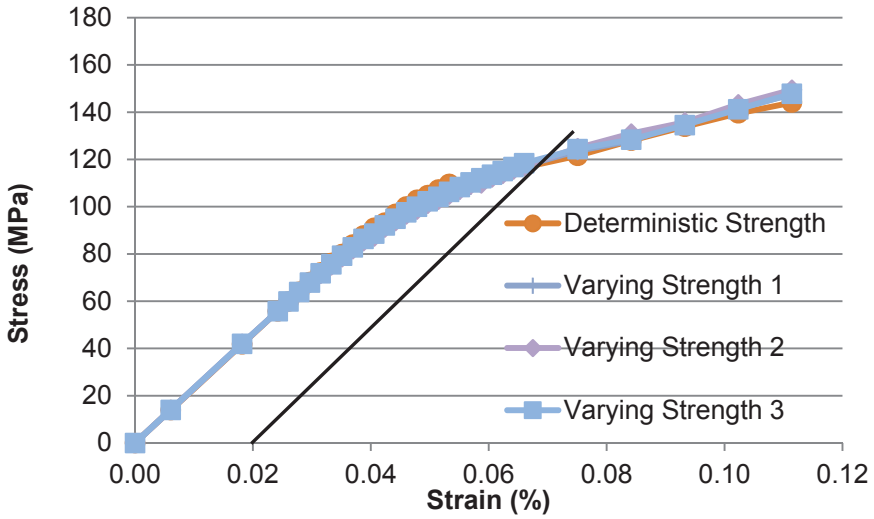

Figure 12. Stress-strain curves of cross section 2 with the deterministic strength and three different sets of strengths drawn from a Weibull distribution

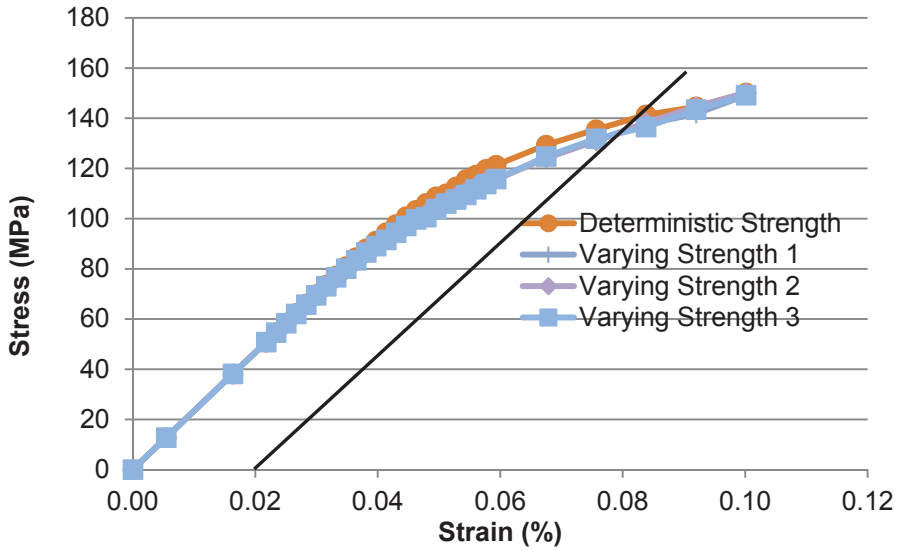

Figure13. Stress-strain curves of cross section 3 with the deterministic strength and three different sets of strengths drawn from a Weibull distribution.

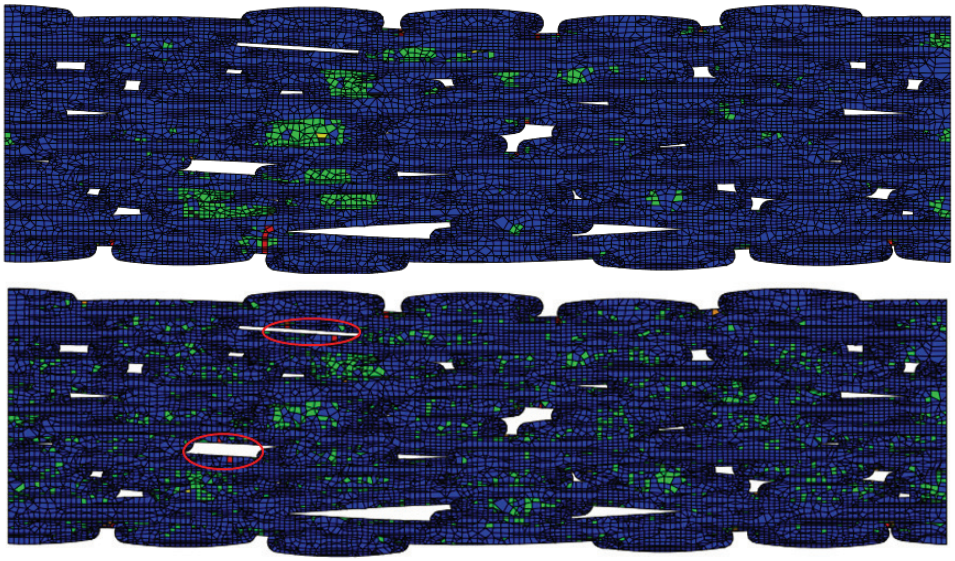

Figure 14. Comparison of damaged area in the deterministic and randomized models of cross section 1

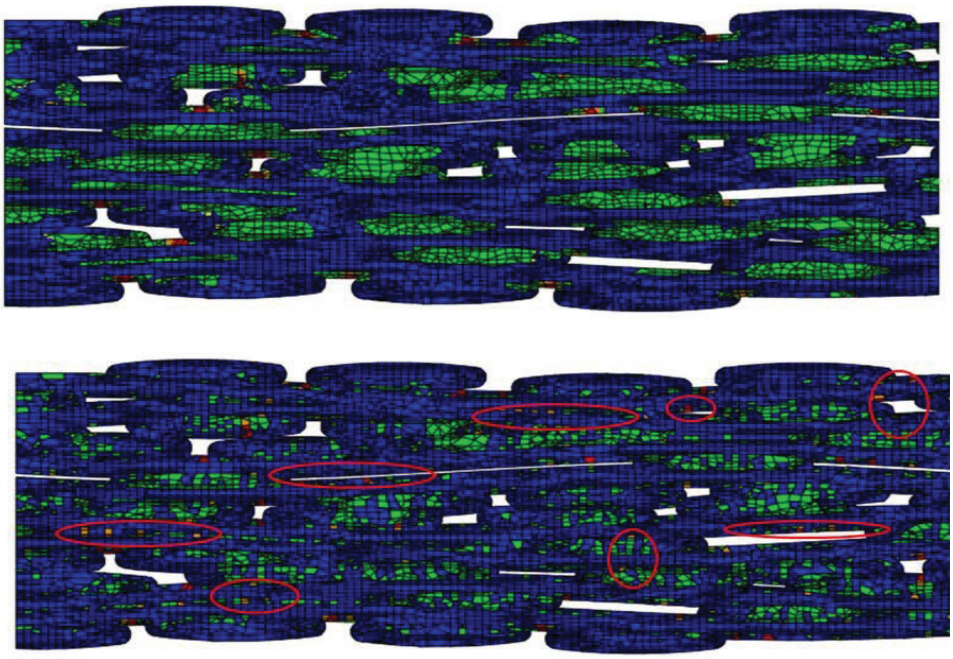

Figure 15. Comparison of damaged area in the deterministic and randomized models of cross section 3

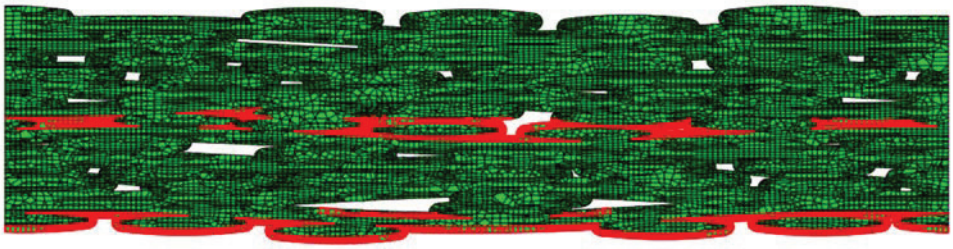

Figure 16. Model with matrix cluster 1 and matrix cluster 5 highlighted in red. The clusters are numbered bottom to top

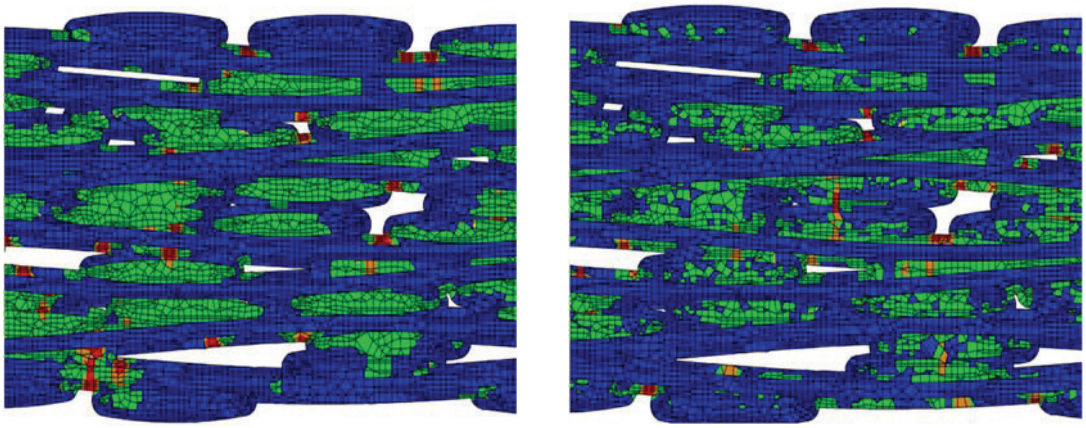

Figure 17. Comparison of randomized model (left) with clustered model (right) in which the clustered model does not fail near one large top void and one large bottom void due to a higher strength in that region

Table 4. Expected change in strength ($\Delta\sigma$) due to a change in mean, compared to the measured change in strength when variable strength used

Mean Matrix Strength (MPa)	Mean Tow Strength (MPa)	Expected $\Delta\sigma$ due to mean (MPa)	$\Delta\sigma$ Section 1 (MPa)	$\Delta\sigma$ Section 2 (MPa)	$\Delta\sigma$ Section 3 (MPa)
247	54.0	-1.0	0.5	1.0	-6.0
254	53.0	3.0	2.5	2.0	-6.0
252	53.0	0.0	0.0	1.0	-5.0

Table 5. Strength in the clusters for the matrix cluster model and tow cluster model. Note that the mean and standard deviation of the strength distributions are the same as that of the randomized model with many clusters

Cluster	Matrix Strength (MPa)	Tow Strength (MPa)
1	213	65
2	293	46
3	254	55
4	223	66
5	177	59
6	144	50
7	248	64
8	316	45
9	314	62
10	293	35
Mean	247	55
St.Dev.	58	10

CONCLUSIONS

From these studies, a few valuable conclusions can be drawn. First, the variability in architecture causes a significant amount of variability in strength (20% difference in strength between the strongest and weakest cross section), especially as compared to the stiffness (less than 5%). Strength is more dependent on local effects than stiffness is, and the voids in the architecture can cause high local stress concentrations. It is not clear what causes the variation in strength between the three architectural models, but should be a topic of future study. What is clear is that variation in the architecture is important to consider.

When the strength is varied randomly throughout the elements of the cross section FE model, there is not a large effect when using the 0.02% offset yield strength. However, when the local strength is grouped into large clusters, more variability in the strength can occur. If there is a region of high stress concentration, met with a large region of relatively strong elements, the composite's strength will be larger than if that area had relatively weak elements. In summary, aspects of the architecture determine how impactful the given local strength will be on the final results. While the architecture causes a larger amount of variability than random constituent strength, the architecture and local constituent strength play a synergistic role in determining the strength of the composite.

ACKNOWLEDGEMENT

The funding for this work was provided by the NASA Graduate Student Research Program, grant number NNX10AM49H. The authors are thankful to Robert Goldberg, Peter Bonacuse, and Subodh Mital of NASA GRC for many helpful discussions.

REFERENCES

[1] F. Desplentere, S. V. Lomov, D. L. Woerdeman, I. Verpoest, M. Wevers, and a. Bogdanovich, "Micro-CT characterization of variability in 3D textile architecture," *Compos. Sci. Technol.*, vol. 65, no. 13, pp. 1920–1930, Oct. 2005.

[2] D. C. Charmpis, G. I. Schuëller, and M. F. Pellissetti, "The need for linking micromechanics of materials with stochastic finite elements: A challenge for materials science," *Comput. Mater. Sci.*, vol. 41, no. 1, pp. 27–37, Nov. 2007.

[3] S. H. Chang, M. P. F. Sutcliffe, and S. B. Sharma, "Microscopic investigation of tow geometry changes in a woven prepreg material during draping and consolidation," *Compos. Sci. Technol.*, vol. 64, no. 10–11, pp. 1701–1707, Aug. 2004.

[4] S. V. Lomov, I. Verpoest, T. Peeters, D. Roose, and M. Zako, "Nesting in textile laminates: geometrical modelling of the laminate," *Compos. Sci. Technol.*, vol. 63, no. 7, pp. 993–1007, May 2003.

[5] K. Woo and J. D. Whitcomb, "Effects of fiber tow misalignment on the engineering properties of plain weave textile composites," *Compos. Struct.*, vol. 31, no. 314, pp. 343–355, 1997.

[6] K. C. Liu and S. M. Arnold, "Impact of Material and Architecture Model Parameters on the Failure of Woven Ceramic Matrix Composites (CMCs) Via the Multiscale Generalized Method of Cells," *NASA/TM-217011*, 2011.

[7] P. J. Bonacuse, S. Mital, and R. Goldberg, "Characterization of the As Manufactured Variability in a CVI SiC/SiC Woven Composite," in *Proceedings of ASME Turbo Expo 2011*, 2011.

[8] M. P. Rao, M. Pantiuk, and P. G. Charalambides, "Modeling the Geometry of Satin Weave Fabric Composites," *J. Compos. Mater.*, vol. 43, no. 1, pp. 19–56, Sep. 2008.

[9] V. Nagpal, M. Tong, P. L. N. Murthy, and S. K. Mital, "Probabilistic Material Sylramic Woven Modeling Fiber / CVI-SiC of High-Temperature Properties Composite of a 5-Harness 0/90 Sylramic Fiber/CVI-SiC/MI-SiC Woven Composite," *NASA Tech. Memo.*, vol. 208497, no. October, 1998.

[10] C. C. Chamis, "Probabilistic Design of Composite Structures," *NASA/TM 2006-214660*, 2006.

[11] H. Zhu, B. B. Sankar, and R. V. Marrey, "Evaluation of Failure Criteria for Fiber Composites Using Finite Element Micromechanics," *J. Compos. Mater.*, vol. 32, no. 8, pp. 766–782, 1998.

[12] R. Jones, *Mechanics of composite materials*, 2nd ed. Philadelphia: Taylor & Francis, 1999.

[13] R. L. Karkkainen, B. V. Sankar, and J. T. Tzeng, "Strength prediction of multi-layer plain weave textile composites using the direct micromechanics method," *Compos. Part B Eng.*, vol. 38, no. 7–8, pp. 924–932, Oct. 2007.

[14] O. Ochoa and J. Engblom, "Analysis of progressive failure in composites," *Compos. Sci. Technol.*, vol. 28, pp. 87–102, 1987.

[15] N. F. Knight, "Factors Influencing Progressive Failure Analysis Predictions for Laminated Composite Structure," pp. 1–25.

[16] D. Blackketter, D. Walrath, and A. Hansen, "Modeling Damage in a Plain Weave Fabric-Reinforced Composite Material," *J. Compos. Technol. Res.*, vol. 15, no. 2, pp. 136–142, 1993.

[17] G. Camus, “Modelling of the mechanical behavior and damage processes of fibrous ceramic matrix composites : application to a 2-D SiC / SiC,” *Int. J. Solids Struct.*, vol. 37, pp. 919–942, 2000.
[18] E. J. Barbero and P. Lonetti, “An Inelastic Damage Model for Fiber Reinforced Laminates,” *J. Compos. Mater.*, vol. 36, no. 8, pp. 941–962, 2002.
[19] A. Puck and H. Schurmann, “Failure analysis of FRP laminates by means of physically based phenomenological models,” *Compos. Sci. Technol.*, vol. 62, pp. 1633–1662, 2002.
[20] E. J. Pineda, A. M. Waas, B. A. Bednarcyk, and C. S. Collier, “Computational Implementation of a Thermodynamically Based Work Potential Model For Progressive Microdamage and Transverse Cracking in Fiber-Reinforced Laminates,” *NASA/TM 2012-217243*, 2012.
[21] R. Talreja, “Transverse Cracking and Stiffness Reduction in Composite Laminates,” *J. Compos. Mater.*, vol. 19, no. 4, pp. 355–375, Jan. 1985.
[22] J. a. Nairn, “The Strain Energy Release Rate of Composite Microcracking: A Variational Approach,” *J. Compos. Mater.*, vol. 23, no. 11, pp. 1106–1129, Nov. 1989.
[23] A. S. D. Wang and F. W. Crossman, “Initiation and Growth of Transverse Cracks and Edge Delamination in Composite Laminates Part 1. An Energy Method,” *J. Compos. Mater.*, vol. 14, no. 1, pp. 71–87, Jan. 1980.
[24] “ABAQUS Software Package, Ver. 6.8, SIMULIA, Providence, RI.” http://www.simulia.com/products/abaqus_fea.html.
[25] A. Hillerborg, M. Modeer, and P.-E. Petersson, “Analysis of Crack Formation and Crack Growth in Concrete by Means of Fracture Mechanics and Finite Elements,” *Cem. Concr. Res.*, vol. 6, pp. 773–782, 1976.
[26] G. I. Barenblatt, “The mathematical theory of equilibrium cracks in brittle fracture,” *Adv. Appl. Mech.*, vol. 7, pp. 55–129, 1962.
[27] Q. Yang and B. Cox, “Cohesive models for damage evolution in laminated composites,” *Int. J. Fract.*, vol. 133, no. 2, pp. 107–137, May 2005.
[28] M. B. Goldsmith, B. V. Sankar, R. T. Haftka, and R. K. Goldberg, “Quantifying Effect of Voids in Woven Ceramic Matrix Composites,” in *54th AIAA/ASME/ASCE/AHS/ASC Structures, Structural Dynamics, and Materials Conference*, 2013.
[29] M. B. Goldsmith, B. V. Sankar, R. T. Haftka, and R. K. Goldberg, “Effects of microstructural variability on thermo-mechanical properties of a woven ceramic matrix composite,” *J. Compos. Mater.*, vol. OnlineFirs, Jan. 2014.
[30] J. Lamon, “A micromechanics-based approach to the mechanical behavior of brittle-matrix composites,” *Compos. Sci. Technol.*, vol. 61, no. 15, pp. 2259–2272, Nov. 2001.
[31] G. Morscher, M. Singh, J. Kiser, M. Freedman, and R. Bhatt, “Modeling stress-dependent matrix cracking and stress–strain behavior in 2D woven SiC fiber reinforced CVI SiC composites,” *Compos. Sci. Technol.*, vol. 67, no. 6, pp. 1009–1017, May 2007.
[32] A. G. Evans and F. W. Zok, “Review The physics and mechanics of fibre-reinforced brittle matrix composites,” *J. Mater. Sci.*, vol. 29, pp. 3857–3896, 1994.
[33] J. Lamon, B. Thommeret, and C. Percevault, “Probabilistic-statistical Approach to Matrix Damage and Stress ± Strain Behavior of 2-D Woven SiC / SiC Ceramic Matrix Composites,” *J. Eur. Ceram.*, vol. 18, pp. 1797–1808, 1998.
[34] Http://www.ceramics.nist.gov/srd/summary/fthexsa.htm, “NIST Property Data Summaries for Hexoloy SA (SiC),” 2001. [Online]. Available: http://www.ceramics.nist.gov/srd/summary/fthexsa.htm. [Accessed: 01-Jan-2013].
[35] Http://www.ceramics.nist.gov/srd/summary/ftgsic.htm, “NIST Property Data Summaries for Silicon Carbide (SiC),” 2001. [Online]. Available: http://www.ceramics.nist.gov/srd/summary/ftgsic.htm. [Accessed: 01-Jan-2013].
[36] S. K. Mital, R. K. Goldberg, and P. J. Bonacuse, “Two-Dimensional Nonlinear Finite Element Analysis of CMC Microstructures,” *Vol. 1 Aircr. Engine; Ceram. Coal, Biomass Altern. Fuels; Wind Turbine Technol.*, pp. 491–496, 2011.

APPENDIX

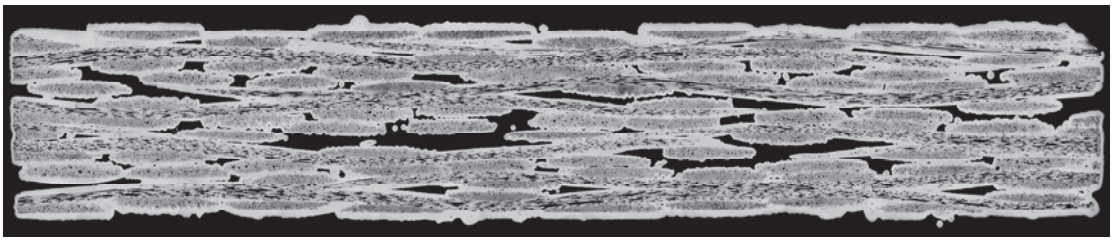

Cross Section 1

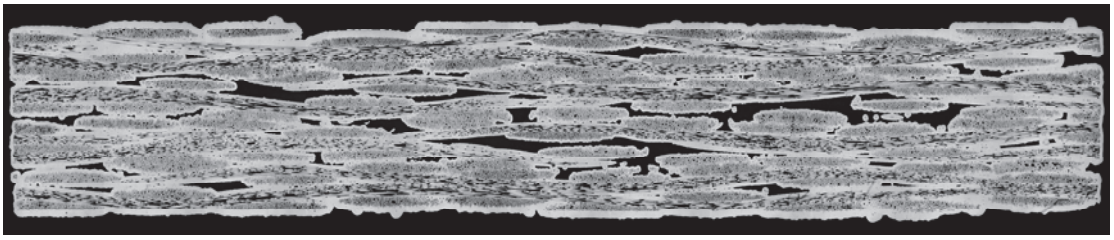

Cross Section 2

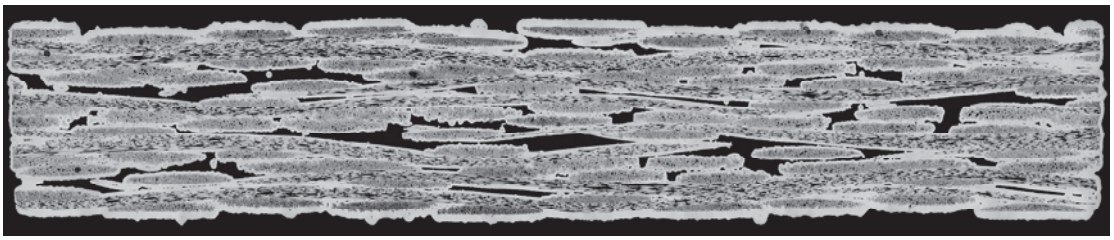

Cross Section 3

Figure A-1. Images of cross sections used for analysis